Bulletin of the Seismological Society of America, Vol. 105, No. 3, pp. –, June 2015, doi: 10.1785/0120140232

Ⓔ

Improved Rapid Magnitude Estimation for a Community-Based, Low-Cost MEMS Accelerometer Network

by Angela I. Chung, Elizabeth S. Cochran, Anna E. Kaiser, Carl M. Christensen, Battalgazi Yildirim, and Jesse F. Lawrence

Abstract Immediately following the M_w 7.2 Darfield, New Zealand, earthquake, over 180 Quake-Catcher Network (QCN) low-cost micro-electro-mechanical systems accelerometers were deployed in the Canterbury region. Using data recorded by this dense network from 2010 to 2013, we significantly improved the QCN rapid magnitude estimation relationship. The previous scaling relationship (Lawrence *et al.*, 2014) did not accurately estimate the magnitudes of nearby (<35 km) events. The new scaling relationship estimates earthquake magnitudes within 1 magnitude unit of the GNS Science GeoNet earthquake catalog magnitudes for 99% of the events tested, within 0.5 magnitude units for 90% of the events, and within 0.25 magnitude units for 57% of the events. These magnitudes are reliably estimated within 3 s of the initial trigger recorded on at least seven stations. In this report, we present the methods used to calculate a new scaling relationship and demonstrate the accuracy of the revised magnitude estimates using a program that is able to retrospectively estimate event magnitudes using archived data.

Online Material: Table of magnitude estimates for Quake-Catcher Network-detected events, and figures clarifying the linear fitting technique used to calculate the Chung *et al.* revised scaling relationship.

Introduction

Earthquake early warning (EEW) systems around the world employ various methods to rapidly calculate earthquake magnitudes using the first few seconds of the seismogram. Typically, the algorithms use amplitude and period information from velocity or, preferably, displacement records (Satriano *et al.*, 2011) For example, the ElarmS network-based early warning system based in California uses a combination of the peak displacement (P_d) and the maximum predominant period (τ_p^{max}) of the P wave (Tsang *et al.*, 2007). Onsite, a single-station system in Taiwan and California, uses P_d and the period parameter τ_c (Wu and Kanamori, 2005; Bose *et al.*, 2009).

Strong shaking from S waves primarily triggers other early warning systems, such as those in Mexico and Taiwan (Espinosa-Aranda *et al.*, 1995; Wu *et al.*, 1998, 2003). For these detections, the stations must delay sending information for several seconds or longer until the strongest shaking is detected. Although these systems generally provide reliable estimates of earthquake magnitude, they are only useful for providing warnings to populations at large distances due to the sizeable blind zone (e.g., area that does not receive advance warning of ground shaking). The system operated by the Central Weather Bureau of Taiwan provides a magnitude estimate approximately 15 s after the P wave arrives at the closest station, which renders the warning useful only to populations greater than 50 km from the epicenter (Wu *et al.*, 1998).

The Quake-Catcher Network (QCN) is a novel seismic network that uses low-cost USB micro-electro-mechanical system (MEMS) accelerometers installed in the homes of volunteers to record earthquakes around the world (Cochran, Lawrence, Christensen, and Chung, 2009; Cochran, Lawrence, Christensen, and Jakka, 2009; Lawrence *et al.*, 2014). In this article, we show that QCN has the potential to provide rapid, low-cost magnitude estimates within the first few seconds for use in early warning systems. The sensors used by QCN are inexpensive (US $30–150), and volunteers provide Internet connectivity and power. Volunteers install and maintain the stations, which minimizes per station costs.

QCN is a unique seismic network that is unlike traditional seismic networks in its use of a relatively small number of highly sensitive seismometers to record earthquakes. QCN implements a very different approach and installs thousands of MEMS sensors around the world for the cost of just a few traditional seismometers and uses them to record earthquakes. The sensors are admittedly lower quality than traditional seismometers and are located in volunteers' homes, schools, offices, and other highly noisy environments. Because

the resulting data are so noisy, with spurious peaks and sometimes strange signals due to the stations' urban environment, we have developed a novel approach to analyze the data. In this study, data from many stations in a small, dense network are averaged to illuminate general trends in the observed acceleration records. These trends are then used to create a revised magnitude scaling relationship that is appropriate for use with noisy QCN data.

A variety of sensors have been used by QCN, including the JoyWarrior24F8 (8-bit), MotionNode (10-bit), JoyWarrior24F14 (14-bit), Onavi (12-bit and 16-bit), and Phidgets (16-bit). The vast majority of sensors currently in use by QCN are 12- to 16-bit JoyWarrior24F14 and Onavi models; the 8- and 10-bit sensors are no longer widely used. QCN uses Berkeley Open Infrastructure for Network Computing (BOINC) (Anderson, 2004) to monitor, record, and transmit data to QCN servers. The stations continuously monitor the sensor accelerations, and, when the accelerations rise above a threshold significance value, a trigger is sent from that station to the server (an in-depth description of the trigger algorithm can be found in Lawrence *et al.*, 2014). The server correlates incoming triggers that occur within 100 s and 200 km of each other. When two or more triggers are correlated, the server estimates the moveout to determine if the propagation speeds match what is expected for an earthquake. When seven or more triggers are correlated, the server calculates a preliminary magnitude and location (additional information about the QCN earthquake location algorithm are found in Chung *et al.*, 2011). For the Christchurch QCN network, the QCN-determined hypocenters are within ~7 km of the GNS reported locations, which in turn have errors on the order of 1 km in latitude and longitude (for more statistics pertaining to the performance of the QCN locations, please see Lawrence *et al.*, 2014). At the time of a detection, a webpage is automatically created on the QCN website that provides the earthquake origin time, location, and magnitude, as well as a map of measured and predicted shaking levels (see Data and Resources). Additional details about the network can be found in Cochran, Lawrence, Christensen, and Chung (2009), Cochran, Lawrence, Christensen, and Jakka (2009), Chung *et al.* (2011), and Lawrence *et al.* (2014).

Since March 2010, the QCN has implemented a real-time detection method to determine the location and magnitude of earthquakes around the world (Chung *et al.*, 2011; Lawrence *et al.*, 2014). A significant advantage of the network is that a very dense array of lower-quality stations can be installed for a fraction of the cost of a traditional seismic network. Even though the stations are of lower quality, the density of stations allows for an earthquake to be quickly detected and verified in near real time. We use a magnitude–distance scaling relationship that is based only on the maximum acceleration at the time of a trigger and at 1, 2, and 3 s after the trigger, respectively. The goal is to provide a reliable magnitude estimate within several seconds of the *P*-wave detection. In Lawrence *et al.* (2014), QCN's rapidly generated AlertMaps are described. These maps are generated using the first 4 s of data following a trigger and are created in approximately 10 s, and thus they can provide predictions of expected peak shaking intensities for locations away from the epicenter. In this study, we chose to focus on rapidly and accurately estimating earthquake magnitudes, as earthquake magnitude and location are used as the basis for warnings issued by current EEW systems implemented globally (e.g., Wu *et al.*, 1998; Wu and Kanamori, 2005; Tsang *et al.*, 2007; Bose *et al.*, 2009). Furthermore, earthquake magnitude is an easily understood measurement for conveying earthquake size to the general public.

The use of acceleration to estimate magnitude is not ideal and does have limitations, including magnitude saturation (Hanks and Johnson, 1976). However, although the QCN data have been shown to be reliable in the estimation of peak ground acceleration and peak ground velocity values (Cochran *et al.*, 2011), it is generally not feasible to integrate lower quality 10–14 bit sensors to displacement, particularly for small-magnitude earthquakes (Evans *et al.*, 2014). However, as MEMS sensors continue to improve in resolution, more complex algorithms could be implemented in the future.

Here, we present an updated magnitude–distance scaling relationship that significantly improves the magnitude estimate used by QCN (Chung *et al.*, 2011; Lawrence *et al.*, 2014). The relationship is derived from aftershock data recorded by QCN stations during the 2010–2013 Canterbury earthquake sequence, New Zealand (Gledhill *et al.*, 2011; Bannister and Gledhill, 2012; Kaiser *et al.*, 2012; Ristau *et al.*, 2013). The previous scaling relationship was developed based on a limited initial dataset; and, while it provided reliable estimates of moderate earthquakes (*M* 4–5.5), it did not perform well across a wider range of magnitudes. The goal of this study is to more accurately estimate earthquake magnitudes using peak ground motions measured within 3 s of the initial trigger.

Data

Immediately following the 2010 *M* 7.2 Darfield, New Zealand, earthquake, over 180 QCN stations were installed in and around the city of Christchurch (see Fig. 1). Most stations are within a 10 km radius of the city center and within approximately 35 km of most aftershocks of the 4 September 2010 *M* 7.2 mainshock, as well as the *M* 6.3 earthquake that followed on 21 February 2011. Complete azimuthal coverage was not possible because sensor sites were limited to locations with available volunteers to host the sensors. Although QCN stations span a variety of site conditions ranging from soft soil to rock, the majority of stations are located on Quaternary alluvium (often relatively stiff at shallow depths) that overlies thick sedimentary sequences forming the Canterbury Plains (Forsyth *et al.*, 2008).

We use data from 185 events detected by QCN stations in and around Christchurch to improve the magnitude scaling relationship (see Data and Resources). The earthquakes occurred from September 2010 to February 2013 and with

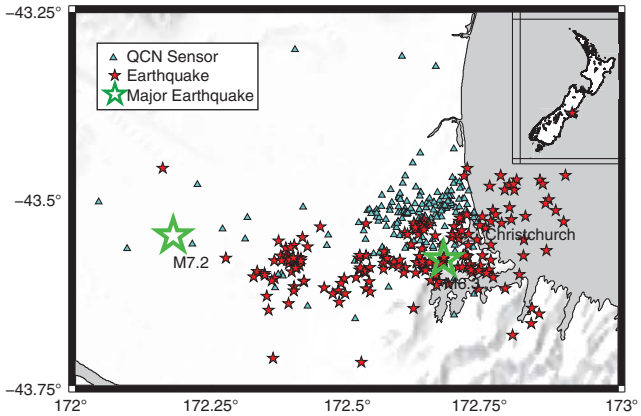

Figure 1. Locations of the Christchurch Quake-Catcher Network (QCN) stations (blue triangles) deployed in September 2010 following the M 7.2 Darfield earthquake and the aftershocks (red and green stars, from the GeoNet catalog) used for this study. The stations are concentrated within the urban center of Christchurch, limiting azimuthal coverage of the earthquake sequence.

magnitudes between M 3.0 and 6.3 as reported in the GeoNet catalog (see Data and Resources). These 185 events are those that were detected by QCN's real-time event detection system. As described in Lawrence *et al.* (2014), many earthquakes that occurred in the Christchurch area were not automatically detected due to the lower resolution of the QCN sensors and the location of the sensors relative to the distribution of earthquakes. Waveforms were recorded at a rate of 50 samples per second. We use 15,063 traces (three components of 5021 station recordings) from 185 earthquakes. QCN-determined hypocentral location estimates for the events examined here were within 10 km of the catalog locations on average (Lawrence *et al.*, 2014). However, here we use GeoNet locations to calculate source–station distances and develop the magnitude–distance scaling relationship.

Methods

We examine how reliably we can estimate earthquake magnitudes using only the first few seconds of acceleration observed at a small number of stations. To develop the scaling relationship, we characterize the general shape of the waveform envelope for the first few seconds following a trigger from the smoothed vector sum of the three components averaged across multiple stations and events.

For each source–station pair, we calculate a mean-removed, average vector sum of the three components of acceleration. We then smooth the traces over a five-point interval. A simple short-term-average/long-term-average standard deviation method is used to identify triggers following the method of Chung *et al.* (2011). Triggers from P- or S-waves are not distinguished; thus, for some traces, the first trigger may be on the S wave. Once a trigger is identified, the smoothed acceleration at the time of the trigger and for 3 s afterward is used to determine a simple empirical magnitude scaling relationship.

We use GeoNet catalog location and magnitude to group the data into bins by station-to-hypocenter distance and magnitude, and the vector sums are averaged for all data in a given bin. The GeoNet catalog estimated location errors are approximately 2 km and magnitude errors are 0.24, on average. The number of traces averaged in each bin is given in Table 1. As expected, the averaged traces for bins with only one or two traces tend to be much more variable than those with many traces, which tend to be smoother. Using a larger number of bins, even though some contained significantly fewer traces than others, created a significantly more robust dataset with which to examine magnitude than using only a few bins with more data in each bin. Also, note that participants were only asked to participate for ~6 weeks during the initial deployment in order to record the early aftershock sequence. At the time of the February 2011 Christchurch event, only 40 ± 10 sensors were still online, limiting the number of waveforms available (Lawrence *et al.*, 2014).

We develop a scaling relationship that uses the source–receiver distance and P_{N_T}, the smoothed and normalized three-component acceleration vector sum at specific times $N_T = 0.02$, 1, 2, and 3 s after a trigger. Here, we use the smoothed vector sum that increases and decreases with time rather than the maximum vector sum that only increases with time as used by Lawrence *et al.* (2014). The trace is normalized by dividing each trace by the three-component vector mean to remove problems such as switched x, y, or z axes (if the sensor was installed upside down, for example) or incorrect station calibration. The smoothed and normalized acceleration values (P_{N_T}) recorded at the time of the trigger ($N_T = 0.02$ s), as well as at times $N_T = 1$, 2, and 3 s after the trigger, are grouped into bins by hypocentral distance (distance bins of 2.5 km between 5 and 20 km, 5 km between 20 and 30 km, 10 km between 30 and 50 km, and a bin from 50 to 70 km, respectively) and then into bins by 0.5 magnitude units between M 2.75 and 6.75 (see Fig. 2, Ⓔ Figs. S1 and S2, available in the electronic supplement to this article). The median values of these bins are then plotted against N_T. Traces from hypocentral distances of less than 5 km or more than 70 km are not used due to lack of data. The amplitudes of each trace show a clear magnitude dependence, and generally decreases with increasing time after the trigger and with increasing hypocentral distance. We fit linear trends to these data to create the magnitude scaling relationship.

We obtain the following magnitude scaling relationship (hereby referred to as Chung *et al.* revised, or CR), in which M is the estimated magnitude, P_{N_T} is the average vector sum of the acceleration at time N_T (number of seconds after the trigger), and d is hypocenter–station distance:

$$M = \frac{\ln(P_{N_T}) - (A_1 N_T d + A_2 d + A_3 N_T + A_4)}{(B_1 N_T d + B_2 d + B_3 N_T + B_4)}, \qquad (1)$$

in which $A_1 = 0.0219$, $A_2 = 0.0244$, $A_3 = -1.92$, $A_4 = -5.82$, $B_1 = -0.00770$, $B_2 = -0.00830$, $B_3 = 0.470$, and $B_4 = 0.311$. This equation is obtained after much experi-

Table 1
Number of Traces per Magnitude and Distance Bin Used to Create Revised Scaling Relationship

	Magnitude Bin							
Distance Bin (km)	2.75–3.25	3.25–3.75	3.75–4.25	4.25–4.75	4.75–5.25	5.25–5.75	5.75–6.25	6.25–6.75
5–7.5	29	113	176	12	15	1	1	2
7.5–10	31	123	427	59	24	4	6	2
10–12.5	6	100	396	141	53	6	9	6
12.5–15	1	50	278	205	57	12	10	2
15–17.5	1	21	246	265	86	27	12	1
17.5–20	1	14	171	263	86	19	10	2
20–25	1	22	191	424	198	22	5	2
25–30	1	10	95	246	116	9	1	1
30–40	1	1	14	112	12	5	4	2
40–50	1	1	1	8	2	3	4	1
50–70	1	1	2	1	2	1	1	2

mentation and is simply a rearranged form of a basic linear equation $y = mx + b$ into $x = (y - b)/m$, with $b(B_1 N_T d + B_2 d + B_3 N_T + B_4)$ and $m(A_1 N_T d + A_2 d + A_3 N_T + A_4)$ found through subsequent linear fits to the data (see Fig. 2, Ⓔ Figs. S1 and S2). We first plot $\ln(P_{N_T})$ versus N_T for all magnitude bins (Fig. 2). In this figure, it is clear that P_{N_T} increases with both increasing time and magnitude bin. Next, we plot $\ln(P_{N_T})$ versus magnitude at the chosen times ($N_T = 0.02$, 1, 2, and 3 s) and find linear fits to the data:

$$\ln(P_{N_T}) = BM + A. \tag{2}$$

Rearranged to solve for magnitude, this becomes

$$M = \frac{\ln(P_{N_T}) - A}{B}. \tag{3}$$

Ⓔ As is shown in Figure S1, the slopes and intercepts of the linear fits vary by both distance (d) and time after the trigger (N_T). In other words, variables A and B in equation (3) are dependent on d and N_T. First, we analyze how the A and B change with d:

$$B = Cd + D \tag{4}$$

and

$$A = Ed + F, \tag{5}$$

in which C, D, E, and F are dummy variables. Values of both the slopes for each magnitude bin versus distance (Ⓔ Fig. S2a) and the intercepts for each magnitude bin versus distance (Ⓔ Fig. S2b) are plotted for each N_T. Linear fits to the data are obtained for each N_T dataset (e.g., red line in Ⓔ Fig. S2). These linear fits provide a slope and an intercept for each N_T value, variables C, D, E, and F, above. The linear fit parameters for both the slope versus distance (Ⓔ Fig. S2a) and intercept versus distance (Ⓔ Fig. S2b) are then plotted by time (Ⓔ Fig. S2c,d). The following equations are created:

$$C = B_1 t + B_2, \tag{6}$$

$$D = B_3 t + B_4, \tag{7}$$

$$E = A_1 t + A_2, \tag{8}$$

and

$$F = A_3 t + A_4. \tag{9}$$

These equations are combined and replaced back into the original formula (equation 3) to obtain equation (1).

To verify these parameters, we ran a bootstrap sampling with replacement algorithm, choosing 185 events at random (with some events from the original dataset repeated and others not used). The bootstrap algorithm is run for 400 iterations, and the following median parameter values are obtained: $A_1 = 0.0235$, $A_2 = 0.0241$, $A_3 = -1.92$, $A_4 = -5.84$, $B_1 = -0.00780$, $B_2 = -0.00830$, $B_3 = 0.470$, and $B_4 = 0.316$. Mean parameter values are $A_1 = 0.0264$, $A_2 = 0.0322$, $A_3 = -1.95$, $A_4 = -5.95$, $B_1 = -0.00830$, $B_2 = -0.00950$, $B_3 = 0.474$, and $B_4 = 0.333$. The standard deviation for each of the parameters is, in the same order, 0.011, 0.025, 0.17, 0.38, 0.0019, 0.0040, 0.031, and 0.064.

We first apply the scaling relationship to an offline code. When testing the new scaling relationship with QCN data, the focus was not on being able to calculate the earthquake magnitude exactly at a single QCN station (because of noisy data), but rather averaging the magnitudes calculated at a small number (minimum of seven) of stations to obtain the correct event magnitude. Magnitudes are estimated for the same 185 events used to develop the new scaling relationship at $N_T = 0.02$, 1.0, 2.0, and 3.0 s after the trigger for each event. We use 15,339 waveforms (again, one per axis for all three axes per station per event), and magnitudes are estimated at all stations for which an automated trigger is identified. To estimate event magnitude, only data from stations with hypocentral distances within 35 km are used (with no

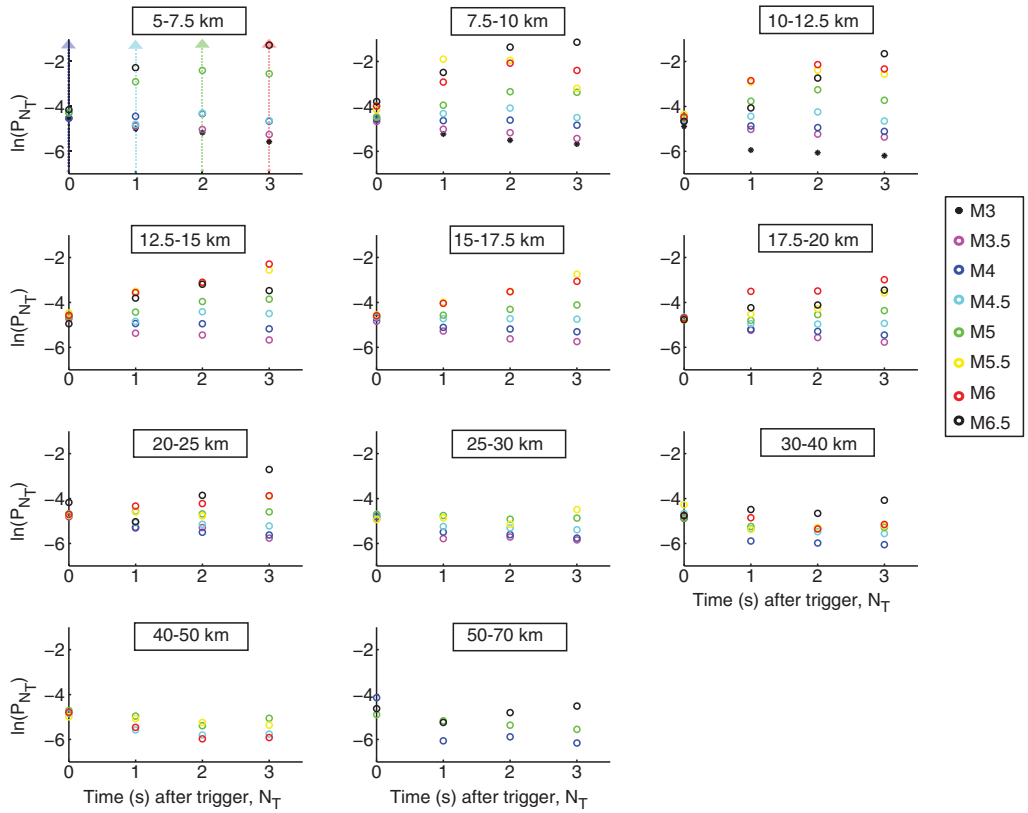

Figure 2. Smoothed acceleration with time averaged by magnitude; magnitude bins are centered around magnitudes 3, 3.5, 4, 4.5, 5, 5.5, 6, and 6.5, and divided into groups by hypocentral distance. The x axis is time in seconds after the trigger (N_T). Number of traces in each distance–magnitude bin can be found in Table 1. The fitted slopes of the averaged accelerations plotted versus earthquake magnitude were used to create the magnitude scaling relationship.

minimum distance requirement), as the scaling relationship appears to be less reliable beyond 35 km, with some magnitude estimates being too high or too low by 2 or more magnitude units. This is perhaps expected due to the fact that the vast majority of the data available to create the scaling relationship were from distances less than 35 km.

When applied retrospectively, the CR scaling relationship results in significantly improved magnitude estimates, particularly at $N_T = 2.0$ and 3.0 s (see Fig. 3). Compared to a mean magnitude estimate error of −1 magnitude units with a standard deviation of 0.39 using Lawrence *et al.* (2014), the new relationship has a mean error of 0.034 magnitude units and a standard deviation of 0.31 when using the peak acceleration 3.0 s after the trigger. Ⓔ Calculated magnitude values for all events can be found in Table S1.

Because we used the same dataset to create and test the scaling relationship, we randomly removed 40 events from the dataset, recalculated the equation parameters using the remaining 145 events, and then applied the new parameters to the limited dataset of 40 events. We required there to be at least one event in each distance–magnitude bin. The mean error for 40 events for all 10 runs of the randomization process was −0.15; the mean standard deviation was 0.36. This is in excellent agreement with the results from using the entire dataset to both create and test the scaling relationship.

To determine the reliability of this updated scaling relationship in the QCN real-time earthquake detection program, we created a pseudo-real-time offline code to rerun the New Zealand dataset. This code, in contrast to the code explained above (which again can use only the data at one N_T time), uses a combination of N_T times, depending on the calculated arrival time of the wave at the station. A preliminary estimate of the earthquake parameters is made at the first detection (this is the first iteration of the event characterization), then as seismic waves move away from the source and additional stations trigger, subsequent estimates of the earthquake location and magnitude are made (additional iterations of the event characterization). As all relevant information (time of trigger, time trigger received at server, acceleration time series associated with a trigger, etc.) is saved on the server, it is possible to simulate the past events to replicate behavior of the real-time system. The offline code is able to simulate the entire dataset of QCN triggers and time-series data (hundreds of gigabytes of data recorded over five years); however, it is a computationally challenging task. The offline code retrieves the trigger data from the database and loads into the memory at 30 min intervals. To accelerate the simulation, the code scans this live memory table every simulated second (usually in several microseconds). A typical simulation of the entire database takes approximately 6 hr to 3 days, de-

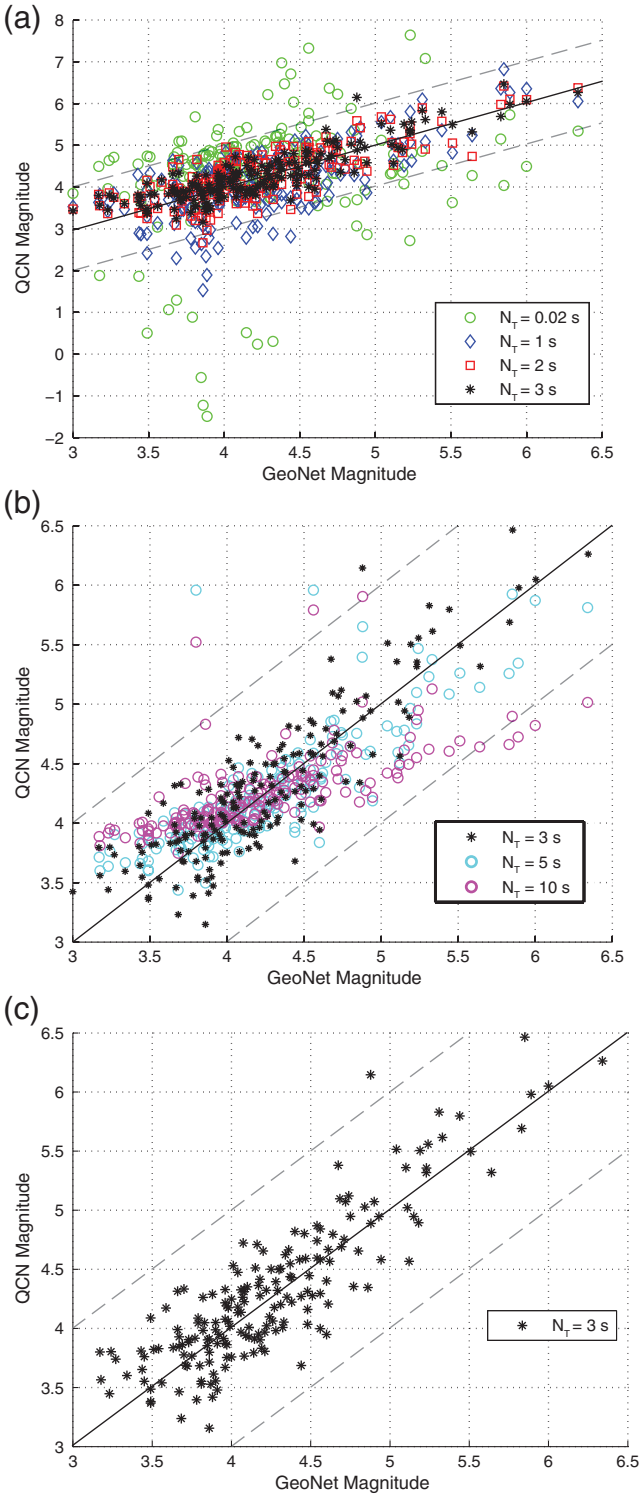

Figure 3. (a) Comparison between magnitudes estimated with the Chung *et al.* revised (CR) magnitude scaling relationship at $N_T = 0.02$, 1, 2, and 3 s, respectively, (b) the CR magnitude estimates at $N_T = 3$, 5, and 10 s, respectively, and (c) results for $N_T = 3$ s only (for the sake of clarity) versus magnitudes from the GeoNet catalog. Here, we use GeoNet catalog locations to determine the source–receiver distance. Dashed lines represent one magnitude unit above and below.

pending on the simulation parameters (such as maximum allowed distance and time for sensors to be correlated). For the purposes of this study, we run the simulation only on the 185 events described above.

The error in the initial magnitude estimates are greater than one magnitude unit in some cases; however, the final iteration is in excellent agreement with both the test run using $N_T = 3$ s, and the GeoNet-reported magnitudes (see Table 2). We note that the final event magnitude may use a combination of N_T times from various stations, depending on characteristics such as the station location and the data transmission latency for a particular station.

To examine the true expected performance, we perform the full offline simulation again, this time using QCN-determined event locations, rather than using the reported GeoNet locations. QCN-determined locations are those reported in Lawrence *et al.* (2014). As shown in Figure 4b, the magnitude estimates are again improved over the previous magnitude–distance scaling relationship, but there are some outliers due to the larger location errors. QCN location estimates varied from GeoNet locations by up to 31 km (a mean of 7.9 km for the dataset used here). Using the QCN-determined locations, we report a mean error of −0.02 and a standard deviation of 0.36. Thus, optimal performance of this scaling relationship within the QCN real-time event detection algorithms will require improvements to the QCN-determined locations. QCN-determined locations are primarily limited by a lack of good azimuthal station coverage of an event, as a large number of the earthquakes occur outside of the densest portion of the QCN array (see Lawrence *et al.*, 2014, for additional details).

We also tested the CR scaling relationship using strong-motion data recorded by traditional seismic stations of the 21 February 2011 M 6.3 Christchurch earthquake. We use data from 10 strong-motion sites operated by GNS Science that were located within 30 km of the earthquake hypocenter. We processed the data and detected triggers in the same way as described above for the QCN data. We do not try to replicate the lower quality of the QCN data, by filtering the data or adding noise, because we want to see if we can get reliable results using higher resolution, traditional strong-motion data. For the Christchurch earthquake, we estimate a magnitude of M 4.4, 6.0, 5.7, and 5.7 at $N_T = 0.02$, 1, 2, and 3 s after the initial trigger at each station, respectively. Using the offline real-time simulation (which uses a combination of N_T times, depending on the wave arrival at the station), the final magnitude estimate is M 5.8. This result is within 0.5 magnitude units of the final GeoNet-reported magnitude and shows that the magnitude–distance scaling relationship developed here may also be useful for traditional strong-motion data. Therefore, it may be possible to combine acceleration data from both traditional strong-motion stations and lower resolution QCN stations in the future to enable faster and more accurate magnitude estimates for EEW systems.

To determine if magnitude estimates would be more robust if we examine a longer segment of the waveform, we recalculate the scaling relationship and corresponding magnitude

Table 2

Comparing the Results of the Offline Simulation for Magnitudes Calculated Using the Lawrence *et al.* (2014) Relationship (Using QCN Hypocentral Locations Only) and the Scaling Relationship Presented in This Study for Both QCN and GeoNet Hypocentral Locations

Locations	Comparison of Offline Simulations					
	Mean Error: Iteration A	Mean Error: Iteration B	Mean Error: Final Iteration	Standard Deviation: Iteration A	Standard Deviation: Iteration B	Standard Deviation: Final Iteration
Lawrence *et al.* (2014) (QCN locations)*	−1.4	−1.4	−1	0.59	0.57	0.39
CR (QCN locations)†	0.23	0.04	−0.023	0.76	0.45	0.36
CR (GeoNet locations)	0.24	0.13	0.03	0.60	0.42	0.31

*QCN, Quake-Catcher Network.

†CR, Chung *et al.* revised scaling relationship.

estimates using $N_T = 5$ and 10 s. The resulting magnitude estimates are worse than those calculated using the CR relationship above. Using $N_T = 5$ s, the mean magnitude difference is 0.096, and the standard deviation is 0.32. Using $N_T = 10$ s, the mean magnitude difference is 0.12 and the standard deviation is 0.57. The poorer performance using longer time segments may be because there is significant background noise at QCN stations, with sometimes only a few seconds of meaningful data observed following a trigger, particularly for especially small or distant events. Thus, we conclude that using shorter time segments is preferable, at least for low signal-to-noise data.

We also tested the performance of the CR relationship developed using 3 s of data (detailed above), but used $N_T =$ 5 and 10 s to estimate the magnitude. However, we noticed no improvements in the resulting magnitude estimates. For $N_T = 5$ s, the mean magnitude estimate error is 0.0083, and the standard deviation is 0.33. For $N_T = 10$ s, the mean error is 0.022, and the standard deviation is 0.43. Although the mean error is lower for $N_T = 5$ s than for the $N_T = 3$ s magnitude estimates, there is a significant deterioration in performance at higher magnitudes (see Fig. 3b).

Discussion

By revising the QCN rapid magnitude scaling relationship, we are able to determine magnitudes to within 0.25 magnitude units of the reported GeoNet magnitude for 55% of the events, within 0.5 magnitude units for ~90% of the events, and to within 1 magnitude unit for all but one of the earthquakes examined in this study (see Table 2). All of the magnitudes are determined with accelerations measured during the first 3 s of the waveforms. Although there are limitations to this relationship, including possible magnitude saturation, the magnitude scaling relationship works well for estimating magnitudes of events that occur within ~35 km of the main station array deployed in Christchurch. The Christchurch dataset provides an excellent case study to validate our methodology for *M* 3–6.3 earthquakes. The applicability of the new scaling relationship in regions subject to different prevailing site conditions or very large magnitude (*M* 7+) events will be investigated as additional data becomes available. It is possible that the CR scaling relationship will need to be tuned to different geologic and/or faulting environments.

We also test the relationship using data recorded by traditional seismometers from the K-NET network for the *M* 6.7 Tottori, Japan, earthquake of 2000. We found that it was only possible to produce reasonable magnitudes using $N_T = 3$ s acceleration values. Using only stations within 35 km, the calculated magnitude was *M* 8.6. Using stations within 20 km, however, reduced the estimated magnitude to *M* 7.2. We suspect that there may be problems when applying revised magnitude scaling relationship to this dataset due to this being a different geologic and faulting environment than the Christchurch aftershock sequence (the Tottori earthquake was ~10 km deep; most earthquakes in the Christchurch area were 5 km deep or less) and the use of only a few sparsely arranged traditional sensors.

Using the acceleration values at the time of the trigger and up to 3 s after a trigger, we are able to rapidly and accurately estimate the magnitude for earthquakes recorded on a dense network of low-cost sensors installed in New Zealand. Estimating the magnitude rapidly, and ideally before shaking has reached population centers, is essential for EEW systems. The use of low-cost sensors to provide a dense set of observations to complement existing seismic networks may speed up development of and improve the performance of EEW systems. A remaining issue is the further improvement of earthquake locations estimated by the low-cost sensors. For the dataset examined here, most of the events were located outside of the area covered by QCN sensors, which led to location estimates with larger errors.

We suggest the use of this scaling relationship for local event-to-station distances only. Because of limited data, we have only been able to sufficiently test the applicability of this relationship to stations with hypocentral distances of less than 35 km, as described above.

Furthermore, as described above, the CR scaling relationship is also limited regarding the earthquake magnitudes that it can estimate. This is a local scaling relationship based on acceleration, so saturation for larger events is probable. Because the magnitude is estimated within 3 s of the trigger, any event that has not ruptured sufficiently by that time will be underestimated. For example, by approxi-

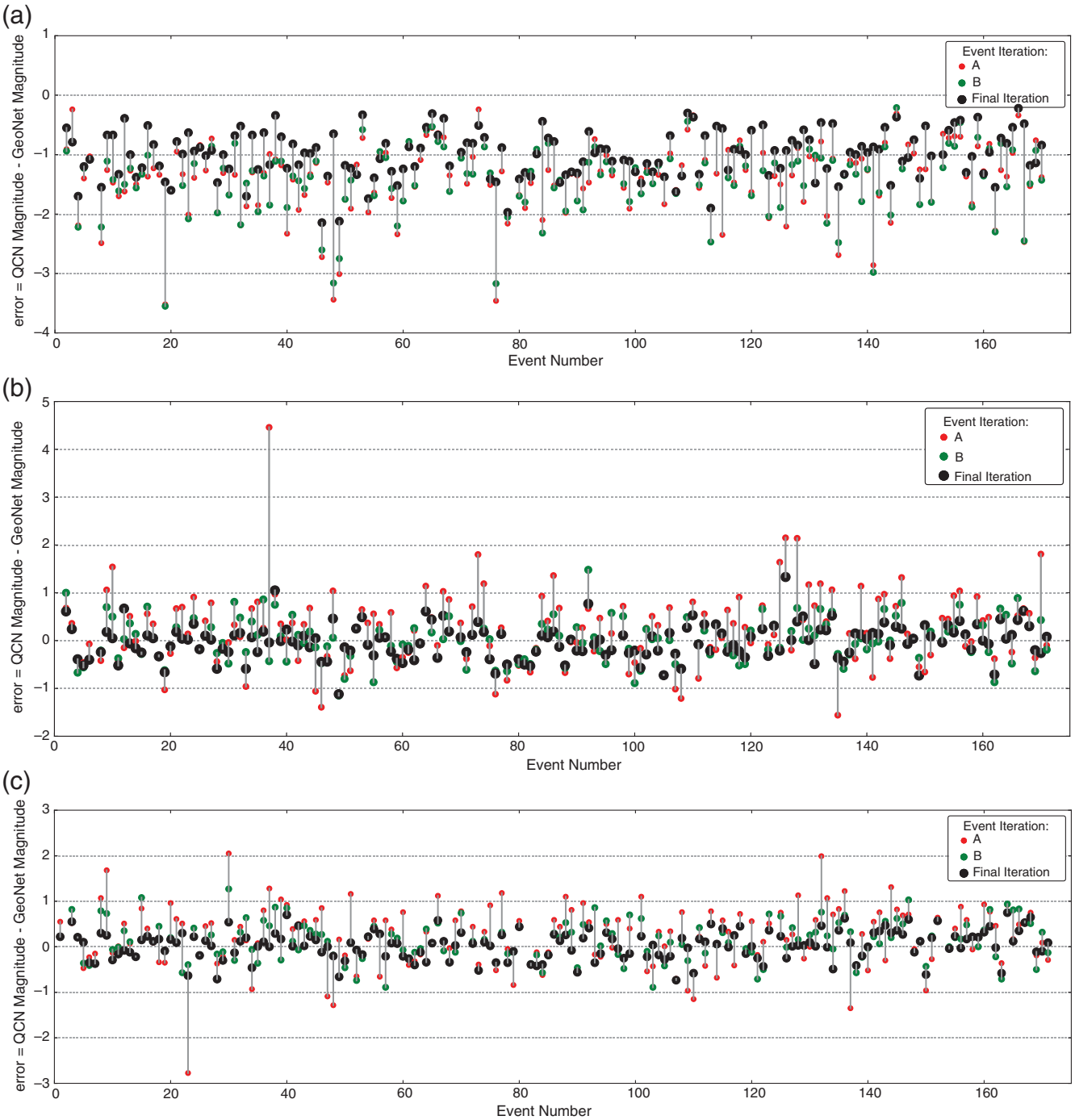

Figure 4. (a) Difference in magnitude between the GeoNet catalog magnitudes and magnitudes estimated by Lawrence *et al.* (2014) using offline simulation. We use QCN-determined locations. Estimates are shown for the first (iteration A), second (iteration B), and final (final iteration) magnitude estimate. The iterations can vary per event depending on how many stations and triggers are used for that event. For the Lawrence *et al.* (2014) scaling relationship, the mean error in the magnitude at the final iteration is −1. (b) Difference in magnitude between the GeoNet catalog and magnitudes estimated with the CR scaling relationship. For the CR scaling relationship using the QCN-determined locations, the mean error of the final iteration is −0.023. (c) The difference in magnitude between the GeoNet catalog and magnitudes estimated using the CR scaling relationship. Here, the GeoNet-reported earthquake locations are used. Other details are the same as in (a). For the CR scaling relationship using the GeoNet locations, the mean error of the final iteration is 0.03.

mating the earthquake rupture as a circular patch (Brune, 1970), assuming a maximum slip of 4 m and a rupture velocity of 3.2 m/s (Kaiser *et al.*, 2012) and using the following equations for rupture time, seismic moment, and moment magnitude (Stein and Wysession, 2007) (equations 10–12, respectively), we can calculate a magnitude M_w 6.2 earthquake

(the revised final magnitude reported for the Christchurch earthquake; Kaiser *et al.*, 2012) has a rupture time of approximately 3.3 s:

$$T_{\mathrm{R}} = L\left(\frac{1}{v_{\mathrm{R}}} - \frac{\cos\theta}{v}\right), \tag{10}$$

$$M_0 = \mu A d, \tag{11}$$

and

$$M_{\mathrm{w}} = \frac{\log(M_0)}{1.5} - 10.73. \tag{12}$$

Larger earthquakes with correspondingly longer rupture times may not have ruptured fully enough for the scaling relationship reported here to be applicable. Hence, for earthquakes larger than $M_{\mathrm{w}} \sim 6.3$, a unique scaling relationship will need to be found. Interestingly, the original Lawrence *et al.* (2014) scaling relationship provides reasonable magnitude estimates for earthquakes at greater distances and for larger events. Thus, it may be possible to combine the original and revised scaling relationships to result in more stable magnitude estimates for larger events.

The revised magnitude scaling relationship presented here will be vitally important to the QCN's rapid magnitude estimations. It will now be possible to calculate earthquake magnitudes within 3 s of the initial trigger with unprecedented accuracy. Not only is this an important study for the QCN team, but, as shown using the GNS data from the Christchurch earthquake, it may be possible to apply this simple magnitude estimation technique to additional networks and datasets. For example, the relationship may also be useful to examine data from earthquakes that are sparsely recorded by QCN or other MEMS accelerometer networks, where it may otherwise be difficult to determine event magnitude. And, although there are currently legal and technical challenges to creating a working EEW system with the QCN, this study shows that with the data provided by QCN in combination with the revised scaling relationship, it is possible to estimate the magnitude of an earthquake both rapidly and accurately.

Data and Resources

All Quake-Catcher Network (QCN) data in this study were collected from the QCN arrays. More information about the QCN and unprocessed data are available at qcn.stanford.edu (last accessed on July 2014). GeoNet data were obtained from the GeoNet earthquake website, geonet.org.nz (last accessed on April 2014).

Acknowledgments

This research was funded by the National Science Foundation Grant EAR 1027913. The authors would like to thank everyone who has helped make the Quake-Catcher Network (QCN) New Zealand deployment possible, particularly GNS, students at the Victoria University of Wellington, and all of the QCN participants. The authors would like to thank our colleagues who provided useful comments to improve the manuscript, including Danielle Sumy and Susan Hough. We would like to thank the two anonymous reviewers who provided helpful comments. Any use of trade, firm, or product names is for descriptive purposes only and does not imply endorsement by the U.S. Government.

References

Anderson, D. P. (2004). BOINC: A system for public-resource computing and storage, *5th IEEE/ACM International Workshop on Grid Computing*, Pittsburgh, Pennsylvania, 8 November 2004.

Bannister, S. C., and K. R. Gledhill (2012). Evolution of the 2010–2012 Canterbury earthquake sequence, *New Zeal. J. Geol. Geophys.* **55,** no. 3, 295–304, doi: 10.1080/00288306.2012.680475.

Bose, M., E. Hauksson, K. Solanki, H. Kanamori, Y.-M. Wu, and T. H. Heaton (2009). A new trigger criterion for improved real-time performance of onsite earthquake early warning in southern California, *Bull. Seismol. Soc. Am.* **99,** no. 2A, doi: 10.1785/0120080034.

Brune, J. N. (1970). Tectonic stress and the spectra of seismic shear waves from earthquakes, *J. Geophys. Res.* **75,** no. 26, 4997–5009.

Chung, A. I., C. Neighbors, A. Belmonte, M. Miller, H. H. Sepulveda, C. Christensen, R. S. Jakka, E. S. Cochran, and J. F. Lawrence (2011). The Quake-Catcher Network rapid aftershock mobilization program following the 2010 M 8.8 Maule, Chile earthquake, *Seismol. Res. Lett.* **82,** no. 4, 526–532.

Cochran, E. S., J. F. Lawrence, C. Christensen, and A. I. Chung (2009). A novel strong-motion seismic network for community participation in earthquake monitoring, *IEEE Instr. Meas.* **12,** 8–15.

Cochran, E. S., J. F. Lawrence, C. Christensen, and R. Jakka (2009). The Quake-Catcher Network: Citizen science expanding seismic horizons, *Seismol. Res. Lett.* **80,** 26–30.

Cochran, E. S., J. F. Lawrence, A. Kaiser, B. Fry, A. I. Chung, and C. Christensen (2011). Comparison between low-cost and traditional MEMS accelerometers: A case study from the M 7.1 Darfield, New Zealand, aftershock deployment, *Ann. Geophys.* **54,** no. 6, doi: 10.4401/ag-5268.

Espinosa-Aranda, J., A. Jiminez, G. Ibarrola, F. Alcantar, A. Aguilar, M. Inostroza, and S. Maldonado (1995). Mexico City seismic alert system, *Seismol. Res. Lett.* **66,** 42–53.

Evans, J. R., R. Allen, A. I. Chung, E. S. Cochran, R. Guy, M. Hellweg, and J. F. Lawrence (2014). Performance of several low-cost accelerometers, *Seismol. Res. Lett.* **85,** no. 1, 147–158, doi: 10.1785/0220130091.

Forsyth, P. J., D. J. A. Barrell, and R. Jongens (2008). Geology of the Christchurch area, Institute of Geological & Nuclear Sciences Limited, Geological Map 16, 1 sheet, GNS Science, Lower Hutt, New Zealand, 67 pp., scale 1:250,000.

Gledhill, K. R., J. Ristau, M. E. Reyners, B. Fry, and C. Holden (2011). The Darfield (Canterbury, New Zealand) M_{w} 7.1 earthquake of September 2010: A preliminary seismological report, *Seismol. Res. Lett.* **82,** 378–386.

Hanks, T. C., and D. A. Johnson (1976). Geophysical assessment of peak accelerations, *Bull. Seismol. Soc. Am.* **66,** no. 3, 959–968.

Kaiser, A. E., C. Holden, J. Beavan, D. Beetham, R. Benites, A. Celentano, D. Collett, J. Cousins, M. Cubrinovski, G. Dellow, *et al.* (2012). The M_{w} 6.2 Christchurch earthquake of February 2011: Preliminary report, *New Zeal. J. Geol. Geophys.* **55,** no. 1, 67–90, doi: 10.1080/00288306.2011.641182.

Lawrence, J. F., E. S. Cochran, A. Chung, A. Kaiser, C. M. Christensen, R. Allen, J. W. Baker, B. Fry, T. Heaton, D. Kilb, *et al.* (2014). Rapid earthquake characterization using MEMS accelerometers and volunteer hosts following the M 7.2 Darfield, New Zealand, earthquake, *Bull. Seismol. Soc. Am.* **104,** no. 1, 184–192, doi: 10.1785/0120120196.

Ristau, J., C. Holden, A. E. Kaiser, C. A. Williams, S. C. Bannister, and B. Fry (2013). The Pegasus Bay aftershock sequence of the M_w 7.1 Darfield (Canterbury), New Zealand earthquake, *Geophys. J. Int.* **195,** no. 1, 444–459, doi: 10.1093/gji/ggt222.

Satriano, C., Y. M. Wu, A. Zollo, and H. Kanamori (2011). Earthquake early warning: Concepts, methods and physical grounds, *Soil Dynam. Earthq. Eng.* **31,** 106–118, doi: 10.1016/j.soildyn.2010.07.007.

Stein, S., and M. Wysession (2007). *An Introduction to Seismology, Earthquakes, and Earth Structure*, Blackwell Publishing, Malden, Massachusetts.

Tsang, L. L. H., R. M. Allen, and G. Wurman (2007). Magnitude scaling relations from *P*-waves in southern California, *Geophys. Res. Lett.* **34,** doi: 10.1029/2007GL031077.

Wu, Y.-M., and H. Kanamori (2005). Experiment on an onsite early warning method for the Taiwan early warning system, *Bull. Seismol. Soc. Am.* **95,** no. 1, 347–353, doi: 10.1785/0120040097.

Wu, Y.-M., T.-C. Shin, and Y.-B. Tsai (1998). Quick and reliable determination of magnitude for seismic early warning, *Bull. Seismol. Soc. Am.* **88,** no. 5, 1254–1259.

Wu, Y.-M., T.-l. Teng, T.-C. Shin, and N.-C. Hsiao (2003). Relationship between peak ground acceleration, peak ground velocity, and intensity in Taiwan, *Bull. Seismol. Soc. Am.* **93,** 386–396.

Stanford University
397 Panama Mall
Mitchell Building 360
Stanford, California 94305
achung@seismo.berkeley.edu
(A.I.C., C.M.C., B.Y., J.F.L.)

U. S. Geological Survey
525 S. Wilson Avenue
Pasadena, California 91106
(E.S.C.)

GNS Science
P.O. Box 30-368
Lower Hutt 5040
New Zealand
(A.E.K.)

Manuscript received 30 July 2014;
Published Online 19 May 2015